Surface & Coatings Technology 364 (2019) 265–272

Contents lists available at ScienceDirect

Surface & Coatings Technology

journal homepage: www.elsevier.com/locate/surfcoat

Anti-wear titanium carbide coating on low-carbon steel by thermo-reactive diffusion

Jin Zhang[a,*], Shuai Li[a], Chenfeng Lu[a], Caiyuan Sun[a], Shuai Pu[a], Qi Xue[a], Yuanhua Lin[a,*], Min Huang[b]

[a] School of Materials Science and Engineering, Southwest Petroleum University, Chengdu 610500, China
[b] Sichuan Bomco Petroleum Drill Bit Co., Ltd, Chengdu 610052, China

ARTICLE INFO

Keywords:
Thermo-reactive deposition
Carburized
Titanizing
Microstructure
Wear resistance

ABSTRACT

In this research, titanium carbide was fabricated onto carburized AISI 1020 steel through thermo-reactive diffusion (TRD) with salt bath processing at 900 °C for 3 h. The researchers investigated the microstructure and the wear resistance of the as-obtained coating. Results showed that the as-received coating was of 7.5 ± 0.3 μm with surface micro-hardness of approximately 1885 ± 121 $HV_{0.025}$. The coating presented excellent adhesion to the substrate as evidenced by a bonding force between the coating (carbide layer) and substrate of approximately 52 N. During the sliding test, its friction coefficient (0.45–0.56) tended to decrease in the final stage. In comparison with the bare substrate, the specific wear volume loss for the titanium carbide–coated specimen decreased by 78%.

1. Introduction

Titanium carbide (TiC) has long been widely used as a coating material for enhancing components' surface properties due to its high melting point, substantial hardness and, strength, and excellent wear resistance, as well as its outstanding chemical stability [1–3]. Such a carbide coating is commonly deposited onto the workpiece by physical vapor deposition (PVD) and chemical vapor deposition (CVD) [4,5]. In recent years, the thermo-reactive deposition process (TRD) has been well established as a good candidate method for both PVD and CVD processes due to its ease of implementation, minimal equipment requirements, and its cost-effectiveness, along with its ability to create the desired adhesion [6–10]. During the TRD process, steels are immersed into a molten salt bath or a series of power pack mixture that contains the relevant carbide forming element (CFE) such as vanadium, niobium, chromium, and molybdenum [11,12]. The metallurgically bonded coating is formed onto the substrate surface as the CFE reacts with the carbon diffused from the substrate, Thus, the carbon content in the steel must be 0.3% or greater in order for the process to guarantee the effective coating thickness and to be commercially viable [13].

Low carbon steel, such as AISI 1020, is widely used in the oil and natural gas industries and chemical and mechanical fields, due to its low cost and strength resistance. However, for some applications in which, outstanding mechanical properties are required, its bulk hardness is not enough to guarantee the best performance. In such applications, the use of TRD treatments that increase surface hardness is an important technological solution for improving tribological properties and the components' life performance. However, untreated low carbon steel cannot be used as the substrate directly due to its limited carbon content. Carburizing is a heat treatment process in which iron or low-carbon steel absorbs carbon while the metal is heated in the presence of a carbon-bearing material. There are two reasons for carburizing low-carbon steel before TRD treatment. First, the carburizing process typically increases the depth of carbon diffusion in order to yield a thick carbide coating during the subsequent TRD process. Moreover, the preliminary-carburizing process is also designed to lower the reaction temperature by promoting the carbon activities [14], and TRD carbide coatings develop at a faster rate by carburizing beforehand [7].

Until now, little data has been available in the literature regarding the duplex titanizing of steels through the TRD process, especially for the salt bath process. In this case, a limited TRD titanizing method was achieved through pack cementation [15]. Furthermore, in salt baths containing borax, a carbide layer can be formed only when the carbide-forming element (CFE) has a low free energy of carbide formation and a relatively high free energy of oxide formation, superior to the B_2O_3 [13,16]. Unfortunately, titanium does not belong to this category [11,17]. Titanium has a smaller energy of oxide formation than B_2O_3,

* Corresponding authors.
E-mail addresses: jzhang@swpu.edu.cn (J. Zhang), yhlin28@163.com (Y. Lin).

https://doi.org/10.1016/j.surfcoat.2019.02.085
Received 1 October 2018; Received in revised form 16 January 2019; Accepted 26 February 2019
Available online 27 February 2019

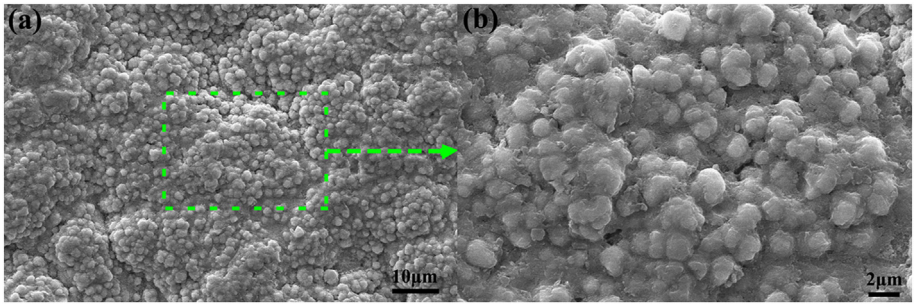

Fig. 1. SEM micrograph of surface morphology of coating on carburized AISI1020 steel.

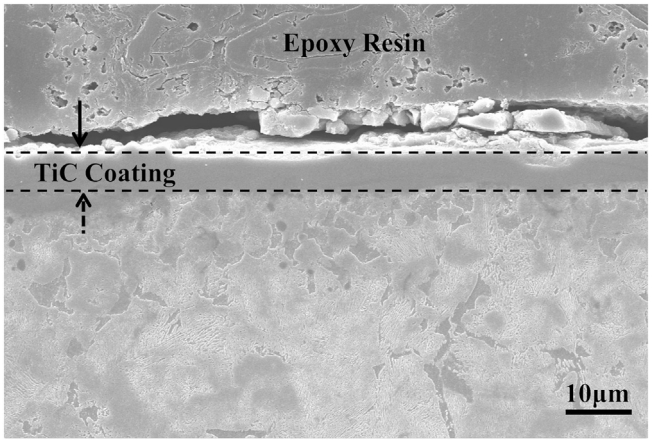

Fig. 2. SEM micrograph of cross-section morphology of coating on carburized AISI1020 steel.

there is an opportunity for boride formation [18]. Thus, it cannot be left free to diffuse and combine with the carbon atoms supplied by the substrate [19].

Therefore, the purpose of this study is to produce a titanium carbide layer on carburized AISI 1020 steel substrate through a TRD method using bath salts, with the aim of extending their use to other industrial applications and gaining a better understanding of the possible applications, benefits and limitations of TRD technology on steel components. The researchers designed and used a neutral salt bath containing $BaCl_2$ and NaCl to eliminate the influence of the commonly used borax salt bath on titanium carbide formation. Aspects of the microstructure of the as-obtained coating and the characteristics of their mechanical response to static and dynamic loads (namely micro-hardness, adhesion and friction behavior) under dry conditions were the focus of the study. The present work will also provide a meaningful reference for the design of duplex coatings and the optimization of processing parameters to meet practical engineering requirements.

2. Materials and experimental method

2.1. Coating fabrication process

AISI 1020 steel was used as the substrate material, which consists of 0.186 C, 0.022 Cr, 0.017 Cu, 0.509 Mn, 0.002 Mo, 0.013 Ni, 0.003 P, 0.030 S, 0.106 Si, and Fe as balance by wt%. The sample was machined to 50 × 15 × 5 mm. The steels were progressively ground and polished by 1200 grit SiC paper. They were then ultrasonically cleaned in

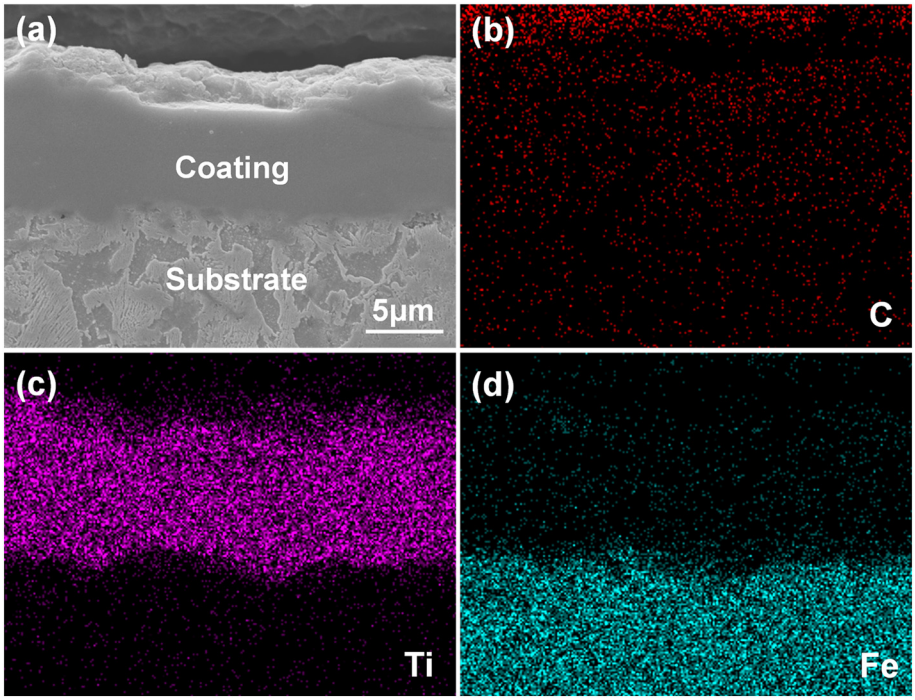

Fig. 3. Cross-sectional elemental mapping obtained from Fig. 2. (a) Secondary electron image morphology with high magnification; (b) carbon element; (c) titanium element; (d) iron element.

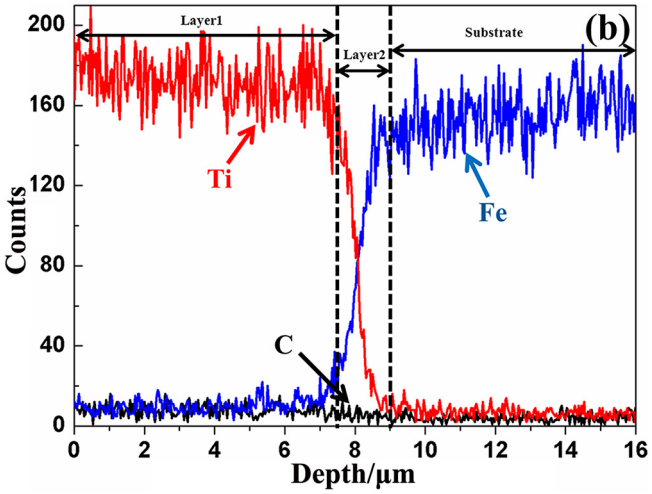

Fig. 4. Corresponding EDS elemental distribution analysis obtained from Fig. 3a.

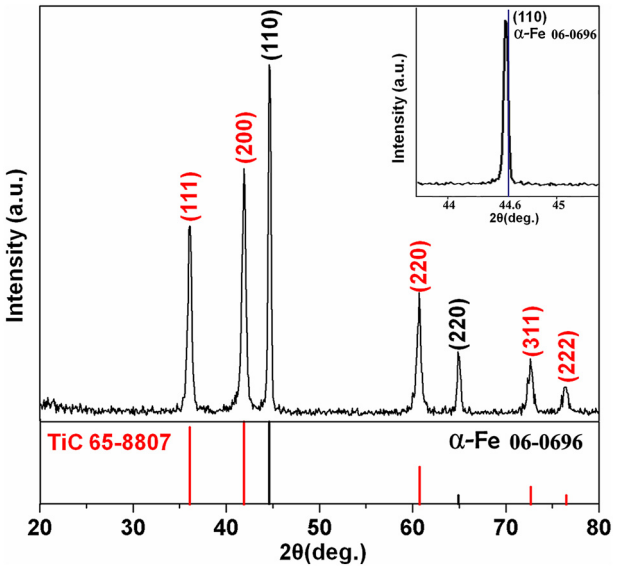

Fig. 5. X-ray diffraction pattern of the titanium carbide coated carburized AISI 1020 steel at 900 °C for 3 h.

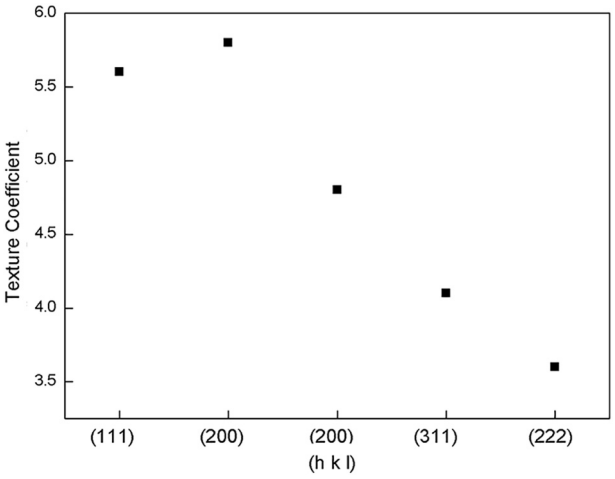

Fig. 6. Texture coefficients of the titanium carbide coating on the AISI 1020 steel at 900 °C for 3 h.

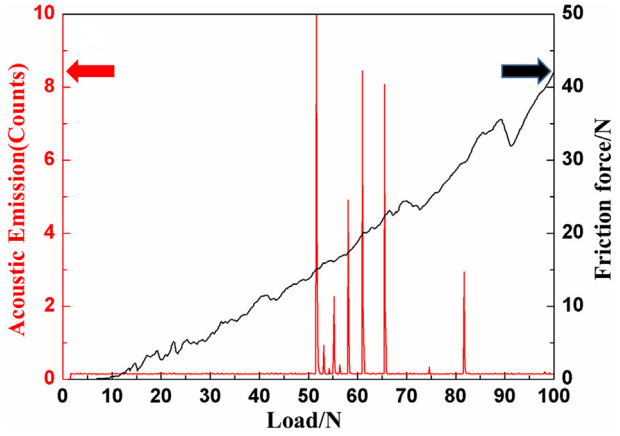

Fig. 7. Acoustic emission and frictional force as a function of applied load in a scratch test of TiC coating onto carburized AISI 1020 steel at 900 °C for 3 h.

acetone, ethanol, and deionised water sequentially for 15 min. The deposition of the TiC coating onto the substrate was completed in two stages. The first step was the gas carburizing process, completed at 950 °C for 15 h with a pressure of 200–300 Pa, with methane (natural gas) as the carburizing medium. The purpose of this step was to enrich the carbon concentration of carbon and improve its activity. The carbon content of the carburizing steel was determined by HCS-140 Infrared Carbon Sulfur Analyzer and the result was about 0.91 wt% near to the steel surface (0.25 mm). The second step was the titanizing process, during which the specimens were immersed in a bath containing 80 wt % neutral salt (base bath) (NaCl: $BaCl_2$ = 3: 7), 10 wt% Ti-Fe powder (Ti: Fe = 3: 7), and 10 wt% NaF (activating agent). The processing temperature and time were set at 900 °C and 3 h, respectively. After the TRD treatment, the samples were removed from the molten bath and subsequent quenched in oil. Finally, the samples were cleaned in boiling water, followed by ultrasonic cleaning in ethanol.

2.2. Characterization

The coating surface and, cross-sectional morphology were investigated by scanning electron microscopy (SEM EVO MA15). For the purpose of cross-section observation, one side of the prepared sample was ground with 1500 mesh SiC paper and polished, then etched with an aqueous solution of 10% potassium hydroxide + 10% potassium ferricyanide (volume fraction). When the thickness of the coating was to be determined on the etched sample, transverse cross sections of at least three samples were polished for examination.

The elemental distribution was characterized by means of an energy-dispersive X-ray spectroscope (EDS) affixed to the microscope. X-ray diffraction (XRD) was performed on the surface of coated samples' using X-ray diffractometer(DX-2000) with Cu Kα radiation (λ = 0.15406 nm)to identify the phase constitution in the coating. The XRD measurements were performed in the 2θ range from 20° to 80° with steps of 0.02°. The X-ray generator was operated at 40 kV and 30 mA.

The micro-hardness of each sample was evaluated using a digital Vickers micro-hardness indenter (DHV-1000), with an applied load of 25 gf and a dwelling time of 15 s. The micro-hardness value was the average of 8 measurements. A homemade MFT-4000 scratch tester was selected to evaluate the adhesive strength between coating and substrates. The measuring parameters were as follows: a loading rate of 100 N/min, a loading scale of 0–100 N, a scratch speed of 10 mm/min, and a traverse distance of 10 mm in ambient air conditions. Both the friction force and acoustic emission signal were automatically recorded when the coatings failed at the adhesive critical loads (L_C). At least three replicates were performed for each sample, and the average

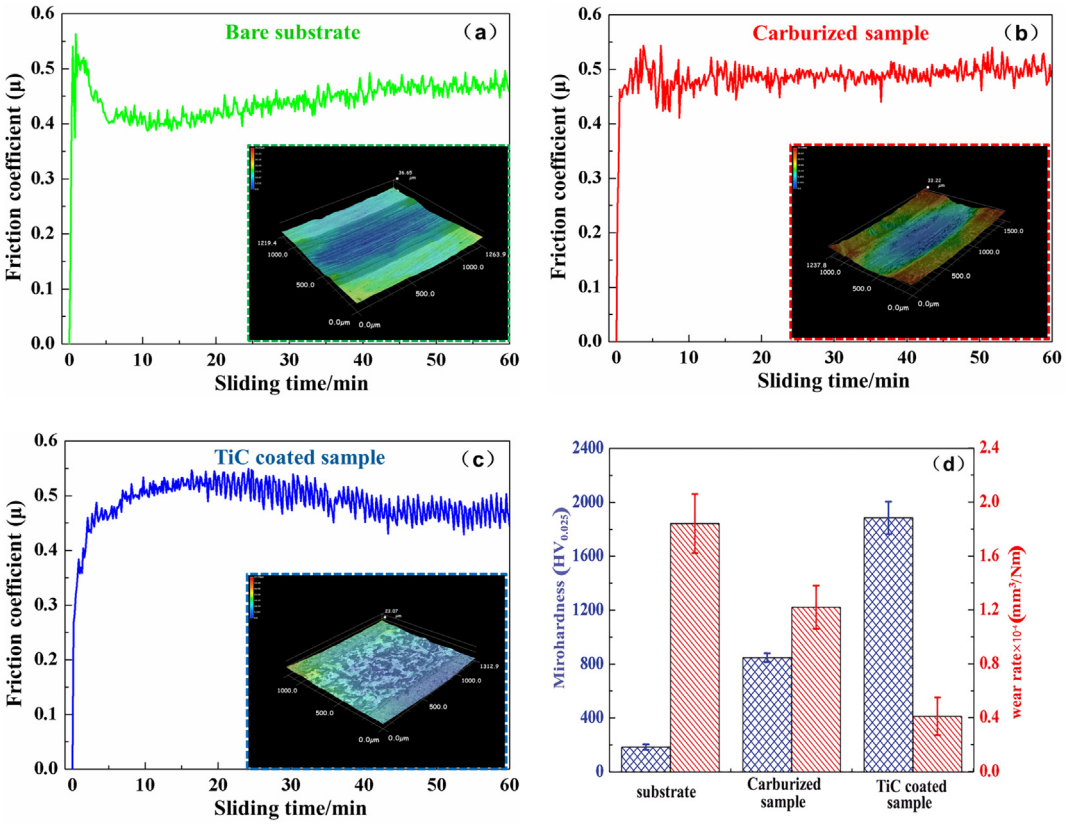

Fig. 8. The evolution of the coefficient of friction of samples, tested at room temperature (a) the bare substrate; (b) carburized matrix; (c) TiC-coated specimen; (d) the micro-hardness and the wear rates of the three samples. The inset in (a), (b) and (c) show the worn surface after test by 3D optical microscopy.

values were recorded.

The tribological properties of the specimens were determined with a homemade MFT-4000 tester with the ball-on-disk technique in linear reciprocated mode. Due to its hardness, excellent corrosion resistance, and high fatigue resistance, AISI 52100 (GCr15) is a good material for mechanical component; thus, AISI 52100 steel ball (835 ± 21 HV0.025) with a diameter of 6.35 mm was used as a counterpart material [13,20]. The ball was fixed and the disk sample slid at a speed of 200 mm/min. The applied constant normal load was 30 N, the wear track length was 15 mm, and the sliding time was 60 min for each test. Worn surfaces were investigated by optical microscopy (DPIXEL520 and KEYENCE VHX-5000 for 2D and 3D morphology, respectively), SEM-EDS. The specific wear rate of the disks (specimens) was determined according to Eq. (1) [21]:

$$K = V/(L \times N) \quad (1)$$

where V is the wear volume loss (mm^3), L is the sliding distance (m), and N is the normal load (N).

The wear volume loss (V) was calculated as:

$$V = S \times D \quad (2)$$

where S is the cross-section area (mm^2), D is the length of the wear scar (mm), S was determined by 3D profile measurements and analysis software (MFT-4000).

3. Results and discussion

Fig. 1 shows the surface morphologies of the obtained specimen coated at 900 °C and 3 h. SEM observation revealed very uniform and fine equiaxed grains, of approximately 0.6–1.0 μm, deposited across the entire surface(Fig. 1b). Fig. 2 illustrates the corresponding cross-sectional morphology of the specimen. It is obvious that the titanium carbide coating (which is verified in Fig. 5) was formed on the surface of the AISI 1020 steel. This layer was approximately 7.5 ± 0.3 μm, and the coating/substrate interface was flat, a result of the outward growth nature of such a coating [22].

Fig. 3 presents the cross-sectional morphology of the as-obtained TiC coating with high magnification and relevant EDS-mapping analysis. As can be seen from Fig. 3a, the TiC layer was continuous, homogenous, and compact, and presented perfect adhesion and consistency with the substrate. Some protrusions enriched with titanium corresponding to the titanium element, were diffused into the steel matrix (Fig. 3c and d).

Accordingly, the mutual diffusion process between titanium, carbon and iron atoms contribute to the cohesion of the interface. The role of the pre-carburizing process is to form a supportive sub-surface for the TiC surface hard layer. This also creates transitional interfacial properties and supplies carbon for the formation of titanium carbide at the surface [7,23].

The details of the inter-diffusion zone are not visible on the SEM micrograph but can be recognized on the Ti and Fe concentration depth profiles measured by EDS elemental distribution analysis (Fig. 4). It shows three distinct zones across the coating. The analysis finds that the titanium was highly enriched in the outermost layer (layer1). Its content stayed nearly stable, indicating the development of a TiC layer, as verified in Fig. 5. Its formation resulted from the atomic reactions of titanium atoms in the thermo-reactive bath with carbon atoms provided by the pre-carburized substrate. In addition, the outermost TiC layer was low in iron, which can be attributed to the limited solid solution of iron in TiC. It is also clear that Ti content decreased gradually while the Fe content increased continually from the surface to the matrix, suggesting that the inter-diffusion between the Ti and the Fe occurred near the interface of the substrate (layer2). Actually, the Fe content increased quickly, moving from the interface to the core of the specimen, and the iron and titanium had a narrow coexistence zone. This layer

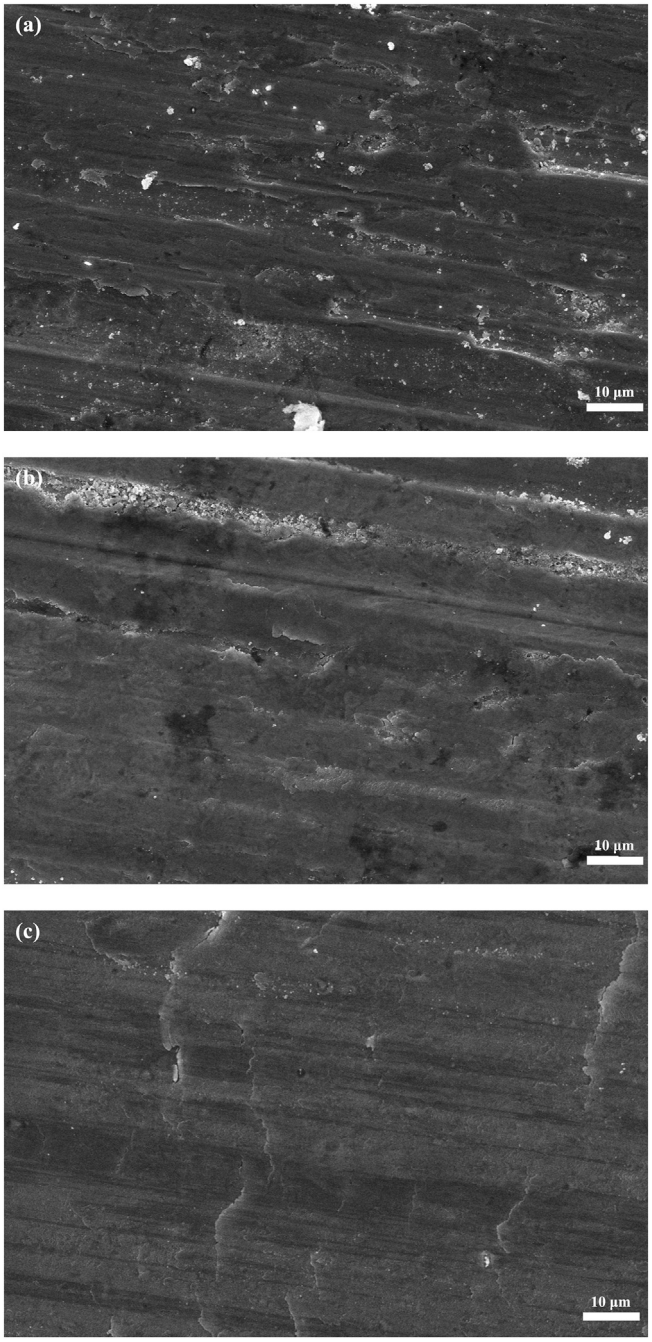

Fig. 9. SEM morphologies of the worn track after dry sliding wear test, (a) the bare substrate; (b) carburized sample and (c) TiC coated specimen.

was mainly composed of iron-titanium solid solution and the titanium concentration dropped quickly at the boundary of solid solution layer and substrate.

This is partly because of the difference scales of titanium and iron atomic radius and the relatively low solubility product of titanium in γ-iron crystal structure at the TRD temperature [24]. A similar observation has been reported for vanadium carbide (VC) coating [25].

Fig. 5 depicts the phase composition of the coated specimen determined by XRD. As presented, the as-obtained coating mainly consisted of TiC (PCPDF 65-8807) and α-Fe (PCPDF06-0696). It indicates that the carbon concentration in the surface region of pre-carburized AISI 1020 steel is sufficient for the growth of carbide layer. The preferred orientation of a certain crystal plane (*h k l*) in the TiC coating was evaluated by the texture coefficient (TC) using the Harris method [25–27]. The ASTM value of the disordered TiC phase was used as the standard value. The calculated TCs (h k l) results are presented in Fig. 6, in which it can be seen clearly that the TCs of (111) and (200) crystal planes were much higher than those of other planes. Therefore, it may be concluded that the TiC coating had the preferred orientations of the (111) and (200) planes. The cause of the preferred orientations and its effects on the coated sample are not clear at present and require further investigation. According to the reaction composition and the Fe-Ti equilibrium phase diagram [28], FeTi and Fe_2Ti phase may not be formed. Due to Ti having a strong chemical affinity for C atoms, it is very easy to form TiC that lowers the solid solubility of Ti in α-Fe [29]. Therefore, only trace titanium atoms are diffused into the matrix during the coating process, thus forming the solid solution of titanium in α-Fe. Furthermore, the reflection peak in the inset of Fig. 5 was shifted slightly to lower angles as compared with the standard α-Fe reflection peaks in the XRD database. This can be attributed to the increment of the crystalline lattice of α-Fe due to the inward diffusion of trace titanium to the substrate.

The diamond stylus was drawn across the coating surface as the applied load increased linearly from 0 to 100 N while the acoustic emission signal and frictional force were recorded. The acoustic emission signal (red line) was found to be an effective mean of determining critical failure loads (L_C) for hard coatings during sliding contact (Fig. 7).

As the applied load increased, the cracks continued to grow until they joined together at L_C and these cracks extended through the scratch width and generated large, sharp acoustic emission levels [30,31]. The scratch test result (Fig. 7) indicated that the, TiC coating was well-adhered to the substrate, exhibiting a high L_C value of approximately 52 N [32]. In fact, TRD method allows for the creation of high adhesion strength of the coating on the workpiece [33]. This, strong adhesion also improves the performance of the coating in term of, wear resistance and corrosion resistance [34].

The ball-on-disk tests allowed us to determine the tribological properties of the as-received specimens. Fig. 8 illustrates the coefficient of friction (COF) as a function of the sliding time for the substrate, carburized, and TiC-coated specimens. All the friction curves showed two typical stages: running-in and steady state. The evolution of the COF, however, differed obviously for each specimen. In the case of the bare substrate (Fig. 8a), after a short running-in stage, its friction curves decreased slightly and then increased continuously. Its worn surface, shown in the inset of Figs. 8a and 9a, showed severe damage with extensive debris and sticking, characteristics of adhesive wear [9]. The counterpart ball (835 $HV_{0.025}$) was much harder than that of the bare substrate (185 $HV_{0.025}$) (Fig. 8d), allowing it to strongly adhere to adhesive junction [35]. During the sliding process, the adhesive junction was sheared, and the adhesion and sliding occurred alternately, resulting in extensive adhesive wear and plastic deformation, thereby increasing the COF.

After the carburizing process, its COF stayed nearly stable with a non-obvious tendency to increase through the whole friction test, as shown in Fig. 8b. The large COF fluctuations in the initial stage may have been the result of ploughing by the asperities of the harder material at the interface of the contact [36]. Its worn morphology, shown in the inset of Figs. 8b and 9b, showed the existence of considerable parallel scratch marks, meaning that abrasive wear dominated. This phenomenon is consistence with the previous studies [37].

For comparison, the TiC-coated specimen presented a relatively long running-in period of approximately 10 min, during which the COF increased gradually. After that, it decreased slowly. As demonstrated in the inset of Figs. 8c and 9c, polishing wear occurred because some fine scratches parallel to the sliding direction were observed in the wear track. The wear track was further characterized through SEM-EDS analysis(Figs. 10 and 11).

Fig. 10a shows the worn micrograph of the TiC coating under the load of 30 N sliding against steel ball counterpart. The coated sample

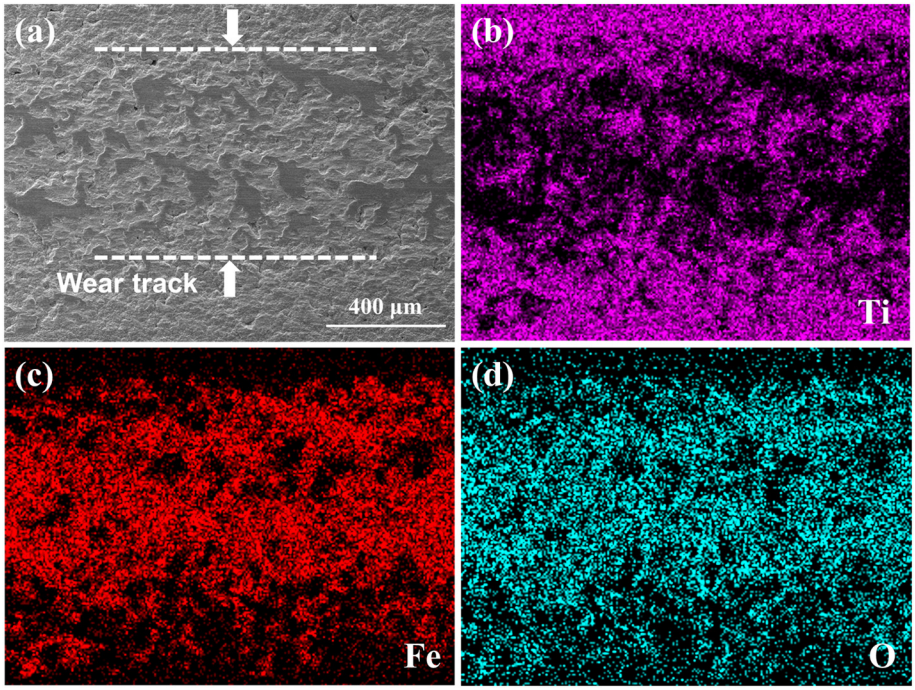

Fig. 10. Worn surface elemental mapping analysis of the titanium carbide coated sample, (a) secondary electron image morphology with high magnification; (b) Ti, element; (c) Fe element; (d) O element.

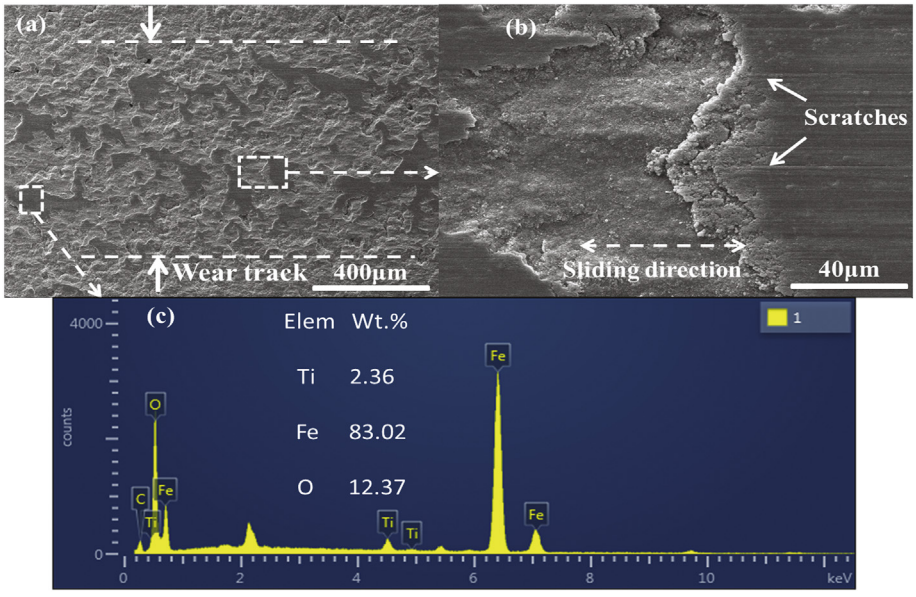

Fig. 11. SEM morphologies of the worn track of the TiC coated sample, (a) wear track; (b) the partial enlarged detail image on the boxed region in Fig. 10a; (c) the EDS element analysis on the boxed region in Fig. 10a.

Table 1
Micro-hardness, wear track depth and the specific wear volume loss for the bare substrate, carburized sample and TiC coated sample.

Specimens	Micro-hardness/$HV_{0.025}$	Wear track depth/μm	Specific wear volume loss $\times 10^{-4}$ (mm^3/N m)
Bare substrate	185 ± 21	11.14	1.84 ± 0.22
Carburized sample	848 ± 32	8.22	1.22 ± 0.16
TiC coated sample	1885 ± 121	2.51	0.41 ± 0.14

showed a dark layer covering some part of the wear track, which seems like the protective oxide layers reported for oxidational wear [38]. The composition analysis obtained by EDX determined that the dark surface layer was rich in oxygen and iron (Figs. 10c, d and 11c), and these two elements were concentrated in the same regions, indicating that dark layer mainly was mainly comprised of iron oxides. In order to compare the results of wear tests to all samples, the micro-hardness, wear track depth and the specific wear volume loss are summarized in Table 1. The

iron, obviously, was most probably transferred from the counterpart the steel ball as the wear depth of the TiC-coated sample was only approximately 2.5 μm, much lower than that of the coating thickness. Furthermore, the worn surface also exhibited minor groves and scratches typical of micro-polishing wear (Fig. 11b).

The main factors affecting the basic wear mechanisms are surface interaction stresses, temperature and oxidation phenomena [39,40]. The higher wear resistance of the TiC- coated sample against the counterpart of steel (Table 1), at lower sliding speeds and intermediate loads (30 N) can be attributed to the load bearing capacity of the TiC coatings. In such conditions, an iron oxide transfer layer forms on the contact surface of the coatings. Actually, the TiC coating may have been oxidized as well. However, it did not appear to have undergone significant tribo-oxidation, and this is possibly due to lower frictional heating in the lower sliding speed and normal load condition [41,42]. These observations are consistent with other findings from the literature [43].

Consequently, the wear process between the steel ball and TiC-coated sample was largely controlled by micro-abrasion of the TiC by oxide particles in the mechanically mixed layer. The wear of the TiC coating was driven by the combination of micro-polishing, micro-abrasion wear and the materials transfer layer. During the sliding process, the Fe adhesion from the GCr15 ball to the TiC coating occurred due to the obvious difference in micro-hardness, causing the increase of the COF in the initial stage [44]. As a result of repeated mechanical stress and frictional heat, Fe atoms react with oxygen to produce iron oxide. Actually, here the formation of titanium oxide seems unlikely. With the formation of some tribo-oxide transfer layers from the steel ball to the TiC layer surfaces, the COF decreased gradually. With respect to the average COF (Table 1), the value for the carburized (0.49) and duplex-treated sample (0.49) was slightly higher than that of the bare substrate (0.44) under the given test condition.

The uncoated steel substrate has the micro-hardness of 185 ± 21 $HV_{0.025}$. The resulting TRD coating greatly enhanced its surface hardness, and the obtained coatings demonstrate a micro-hardness of 1885 ± 121 $HV_{0.025}$ (Table 1). The lower hardness of the TiC coating in our study in comparison with that given in other literature can be related to its lower compaction and thickness [45] since, there were some micro-cracks on the obtained coating surface (see Fig. 1). In addition, micro-hardness measurements of the coatings are usually influenced by the steel matrix. For static measurements the load must be high enough to produce an indentation easy to measure using an optical microscope. Usually this requirement extends the plastic deformation zone into the substrate; thus, the result is a combination of coating and substrate [46,47]. The improvement of the micro-hardness reduces the number of dislocation movements and enhances the plastic deformation resistance, thereby effectively minimizing wear volume loss. In relation to the bare substrate, the specific wear volume loss for the carburized sample and the TiC-coated specimen decreased by 34% and 78%, respectively.

4. Conclusions

Anti-wear titanium carbide coating was successfully adhered onto the carburized AISI 1020 steel by thermo-reactive diffusion at 900 °C for 3 h, comprising a homogenous carbide layer with 7.5 ± 0.3 μm thickness, and a flat interface was formed between the coating and the substrate. A narrow inter-diffusion region of titanium (from TRD) and iron was located beneath the carbide layer, favoring the cohesion of the interface and promoting the transition of physical properties. In comparison with the bare substrate and the carburized sample, the wear resistance of the TiC-coated specimen was greatly enhanced.

Acknowledgement

This work was supported by the China Scholarship Council (Grant No. 201608515034), the Youth science and technology innovation team of electrochemistry for energy materials (Southwest Petroleum University, No. 2015CXTD04), and the Key Lab of Material of Oil and Gas Field (Southwest Petroleum University, Grant No. X151518KCL25).

References

[1] S. Cho, I. Jo, Y.H. Lee, Y.W. Yoo, E. Byon, S.K. Lee, S.B. Lee, Highly improved oxidation resistance of TiC-SKD_{11} composite by SiC/TiB_2 based hybrid coating, Appl. Surf. Sci. 448 (2018) 407–415.
[2] S.J. Algodi, J.W. Murray, M.W. Fay, A.T. Clare, P.D. Brown, Electrical discharge coating of nanostructured TiC-Fe cermets on 304 stainless steel, Surf. Coat. Technol. 307 (2016) 639–649.
[3] M. Yang, Z. Guo, S. Zhang, H. Du, J. Long, K. Qiu, Liquid phase sintering-based coating of Al_2O_3/TiC composite layer on cemented carbide, Mater. Lett. 162 (2016) 146–149.
[4] N. Kumar, G. Natarajan, R. Dumpala, R. Pandian, A. Bahuguna, S.K. Srivastava, T.R. Ravindran, S. Rajagopalan, S. Dash, A.K. Tyagi, R.M.S. Ramachandra, Microstructure and phase composition dependent tribological properties of TiC/a-C nanocomposite thin films, Surf. Coat. Technol. 258 (2014) 557–565.
[5] J. Zhang, Q. Xue, S. Li, Microstructure and corrosion behavior of TiC/Ti (CN)/TiN multilayer CVD coatings on high strength steels, Appl. Surf. Sci. 280 (2013) 626–631.
[6] G. Khalaj, A. Nazari, S.M.M. Khoie, M.J. Khalaj, H. Pouraliakbar, Chromium carbonitride coating produced on DIN 1.2210 steel by thermo-reactive deposition technique: thermodynamics, kinetics and modeling, Surf. Coat. Technol. 225 (2013) 1–10.
[7] H. Pouraliakbar, G. Khalaj, L. Gomidželović, M.J. Khalaj, M. Nazerfakhari, Duplex ceramic coating produced by low temperature thermo-reactive deposition and diffusion on the cold work tool steel substrate: thermodynamics, kinetics and modeling, Ceram. Int. 41 (2015) 9350–9360.
[8] X. Su, S. Zhao, J. Hou, G. Yu, Y. Chen, H. Sun, P. Zhang, L. Xie, Formation of chromium carbide coatings on HT250 steel by thermal diffusion processes in fluoride molten salt bath, Vacuum 155 (2018) 219–223.
[9] C. Sun, Q. Xue, J. Zhang, S. Wan, A.K. Tieu, Bach H. Tran, Growth behavior and mechanical properties of Cr-V composite surface layer on AISI D3 steel by thermal reactive deposition, Vacuum 148 (2018) 158–167.
[10] Q.Y. Wang, Y. Behnamian, H. Luo, X.Z. Wang, M. Leitch, H. Zeng, J.L. Luo, Anticorrosion performance of chromized coating prepared by pack cementation in simulated solution with H_2S and CO_2, Appl. Surf. Sci. 419 (2017) 197–205.
[11] T. Arai, H. Fujita, Y. Sugimoto, Y. Ohta, Diffusion carbide coatings formed in molten borax systems, J. Mater. Eng. 9 (1987) 183–189.
[12] Q. Xue, C. Sun, J.Y. Yu, L. Huang, J. Wei, J. Zhang, Microstructure evolution of a Zn-Al coating co-deposited on low-carbon steel by pack cementation, J. Alloys Compd. 699 (2017) 1012–1021.
[13] C.K.N. Oliveira, C.L. Benassi, L.C. Casteletti, Evaluation of hard coatings obtained on AISI D2 steel by thermo-reactive deposition treatment, Surf. Coat. Technol. 201 (2006) 1880–1885.
[14] B. Chicco, W.E. Borbidge, E. Summerville, Experimental study of vanadium carbide and carbonitride coatings, Mater. Sci. Eng. A 266 (1999) 62–72.
[15] U. Sen, Kinetics of titanium nitride coatings deposited by thermo-reactive deposition technique, Vacuum 75 (2004) 339–345.
[16] B. Mattia, Vincenzo M. Sglavo, Chromium and vanadium carbide and nitride coatings obtained by TRD techniques on UNI 42CrMoS4 (AISI 4140) steel, Surf. Coat. Technol. 286 (2016) 319–326.
[17] T. Arai, Carbide coating process by use of molten borax bath in Japan, J. Heat Treating 1 (1979)16–22.
[18] F.E. Castillejo, J.J. Olaya, J.M. Arroyo-Osorio, Nb-Cr complex carbide coatings on AISI D2 steel produced by the TRD process, J. Braz. Soc. Mech. Sci. Eng 37 (2015) 87–92.
[19] C.K.N. Oliveira, R.M. Muñoz Riofano, L.C. Casteletti, Formation of carbide layers on AISI H13 and D2 steels by treatment in molten borax containing dissolved both Fe–Nb and Fe–Ti powders, Mater. Lett. 59 (2005) 1719–1722.
[20] R.H. Zhang, L.P. Wang, Synergistic improving of tribological properties of amorphous carbon film enhanced by F-Si-doped multilayer structure under corrosive environment, Surf. Coat. Technol. 276 (2015) 626–635.
[21] N.E. Beliardouh, C. Nouveau, M.J. Walock, P. Jacquet, A study of the wear performance of duplex treated commercial low-alloy steel against alumina and WC balls, Surf. Coat. Technol. 259 (2014) 483–494.
[22] X.S. Fan, Z.G. Yang, Z.X. Xia, C. Zhang, H.Q. Che, The microstructure evolution of VC coatings on AISI H13 and 9Cr18 steel by thermo-reactive deposition process, J. Alloys Compd. 505 (2010) L15–L18.
[23] M. Aghaie-Khafri, F. Fazlalipour, Kinetics of V(N,C) coating produced by a duplex surface treatment, Surf. Coat. Technol. 202 (2008) 4107–4113.
[24] S. Nakamichi, S. Tsurekawa, Y. Morizono, T. Watanabe, M. Nishida, A. Chiba, Diffusion of carbon and titanium in γ-iron in a magnetic field and a magnetic field gradient, J. Mater. Sci. 40 (2005) 3191–9198.
[25] X.S. Fan, Z.G. Yang, C. Zhang, Y.D. Zhang, H.Q. Che, Evaluation of vanadium carbide coatings on AISI H13 obtained by thermo-reactive deposition/diffusion technique, Surf. Coat. Technol. 205 (2010) 641–646.
[26] Y.M. Chen, G.P. Yu, J.H. Huang, Role of process parameters in the texture evolution of TiN films deposited by hollow cathode discharge ion plating, Surf. Coat. Technol. 141 (2001) 156–163.
[27] Y. Wang, Z.X. Song, D.Y. Ma, X.Y. Wei, K.W. Xu, Crystalline orientation and surface

structure anisotropy of annealed thin tungsten films, Surf. Coat. Technol.201(2007) 5518.
[28] H. Max, K. Anderko, H.W. Salzberg, Constitution of binary alloys, J. Electrochem. Soc. 105 (1958) 260C–261C.
[29] S. Akamatsu, M. Hasebe, T. Senuma, Y. Matsumura, O. Kisue, Thermodynamic calculation of solute carbon and nitrogen in Nb and Ti added extra-low carbon steels, ISIJ Int. 34 (1994) 9–16.
[30] F. Davanloo, C.B. Collins, K.J. Koivusaari, Scratch adhesion testing of nanophase diamond coatings on steel and carbide substrates, J. Mater. Res. 14 (1999) 3474–3482.
[31] K. Farokhzadeh, A. Edrisy, G. Pigott, P. Lidster, Scratch resistance analysis of plama-nitrided Ti-6Al-4V alloy, Wear 302 (2013) 845–853.
[32] B. Casas, U. Wiklund, S. Hogmark, L. Llanes, Adhesion and abrasive wear resistance of TiN deposited on electrical discharge machined WC-Co cemented carbides, Wear 265 (2008) 490–496.
[33] T. Arai, The thermo-reactive deposition and diffusion process for coating steels to improve wear resistance, Thermochemical Surface Engineering of Steels (2015) 703–735.
[34] S. Hogmark, S. Jacobson, M. Larsson, Design and evaluation of tribological coatings, Wear 246 (2000) 20–33.
[35] L. Liu, H.H. Shen, X.Z. Liu, Q. Guo, T.X. Meng, Z.X. Wang, H.J. Yang, X.P. Liu, Wear resistance of TiN (Ti2N)/Ti composite layer formed on C17200 alloy by plasma surface Ti-alloying and nitriding, Appl. Surf. Sci. 388 (2016) 103–108.
[36] O.A. Gómez-Vargas, J. Solis-Romero, U. Figueroa-López, M. Ortiz-Domínguez, J. Oseguera-Peña, A. Neville, Boro-nitriding coating on pure iron by powder-pack boriding and nitriding processes, Mater. Lett. 176 (2016) 261–264.
[37] M. Izciler, M. Tabur, Abrasive wear behavior of different case depth gas carburized AISI 8620 gear steel, Wear. 260 (2006) 90–98.
[38] T.F.J. Quinn, Review of oxidational wear, Part I: the origins of oxidational wear, Tribol. Int. 16 (1983) 257–271.
[39] E. Rabinowicz, Friction and Wear of Materials, John Wiley and Sons, Inc., New York, 1995, pp. 124–143.
[40] G. Rasool, S. Mridha, M.M. Stack, Mapping wear mechanisms of TiC/Ti composite coatings, Wear 328-329 (2015) 498–508.
[41] P.K. Ajikumar, M. Kamruddin, T.R. Ravindran, S. Kalavathi, A.K. Tyagi, Oxidation behavior of TiC_XN_{1-x} coatings as a function of C/N ratio, Ceram. Int. 40 (2014) 10523–10529.
[42] G. Rasool, M.M. Stack, Wear maps for TiC composite based coatings deposited on 303 stainless steel, Tribol. Int. 74 (2014) 93–102.
[43] S. Wilson, A.T. Alpas, Wear mechanism maps for TiN-coated high speed steel, Surf. Coat. Technol. 120-121 (1999) 519–527.
[44] F. Fernandes, T. Polcar, A. Cavaleiro, Tribological properties of self-lubricating TiSiVN coatings at room temperature, Surf. Coat. Technol. 267 (2015) 8–14.
[45] H. Holleck, Material selection for hard coatings, J. Vac. Sci. Technol. A 4 (1986) 2661–2669.
[46] F. Hakami, M. Heydarzadeh Sohi, J. Rasizadeh Ghani, Duplex surface treatment of AISI 1045 steel via plasma nitriding of chromized later, Thin Solid Films 519 (2011) 6792–6796.
[47] Y. Wang, T.M. Zhang, W.M. Zhao, X.Y. Tang, Sealing treatment of aluminum coating on s235 steel with thermal diffusion of zinc, J. Therm. Spray Techn. 24 (2015) 1052–1059.